CHAPTER 1

General Introduction

General Introduction

In about 30-50 % of enzymes nature utilizes transition metal ions as part of the active site to realize biological catalysis (Hill *et al.* 1999; Kaim *et al.* 2004). Such enzymes are denoted as metalloenzymes. An important class of metalloenzymes termed "hydrogenase" (Stephenson *et al.* 1931) is able to catalyze the reversible heterolytic cleavage of molecular hydrogen (Equation 1) .

$$H_2 \Leftrightarrow 2H^+ + 2e^- \tag{1}$$

Hydrogenases are found in a variety of microorganisms, mostly in prokaryotes, but also in certain eukaryotes like green algae, protozoa, and fungi (Lenz *et al.* 2001; Vignais *et al.* 2001) (see Fig. 1). Hydrogenase-containing microorganisms predominantly live under anaerobic conditions. The hydrogenases play a central role in their energy household (Cammack 1999). Like their hosts, hydrogenases mostly are highly sensitive to dioxygen (O_2) (Cammack *et al.* 2001) (see also Fig. 4). In anaerobic biotopes, microbes release hydrogen as a result of fermentation of organic matter or as a side-product in the course of nitrogen fixation (Lenz *et al.* 2002). Such H_2 is employed as an electron source by H_2ase-containing organisms to generate reducing equivalents, e. g., for CO_2 fixation.
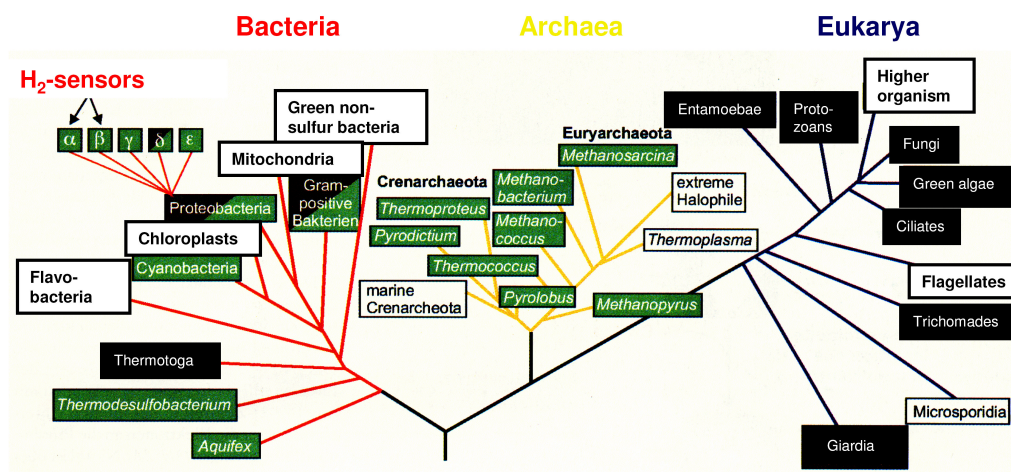

Figure 1: Phylogenetic tree showing the relationships and distribution of hydrogenases among the major phyla (adapted from (Lenz *et al.* 2001)). In various organisms, Ni-Fe H_2ases (green fields) and Fe-only H_2ases (black fields) have been found. H_2-sensing hydrogenases have been observed only in α and β proteobacteria. For more detailed information about hydrogenase containing organisms see (Adams *et al.* 1981).

All hydrogenases are metalloenzymes which contain metal ions in their active site. Besides of the metallic active site, most hydrogenases contain several Fe-S clusters of different types and further redox active species, which may be involved in the electron transfer reactions. Hydrogenases can be classified according to their metal content of the active site (Fig. 2).

Ni-Fe H$_2$ases: Ni-Fe hydrogenases are the largest and best characterized group of hydrogenases, containing a Ni-Fe active site (Przybyla *et al.* 1992; Albracht 1994) (Fig. 1, green fields and Fig. 2). Ni-Fe hydrogenases show a preference for H$_2$ oxidation rather than production. A subfamily, denoted as Ni-Fe-Se hydrogenases, holds additionally one selenium from seleno-cysteine in the active site (Garcin *et al.* 1999). The Ni-Fe hydrogenases of *Ralstonia eutropha* are the main subject of this thesis.

Fe-Fe H$_2$ases: Iron-only (Fe-Fe) hydrogenases (Adams 1990), contain a bimetallic iron core in the active site (Fig. 1, black fields and Fig. 2). Fe-Fe H$_2$ases are evolutionarily unrelated to Ni-Fe hydrogenases. Compared to Ni-Fe hydrogenases, Fe-Fe hydrogenases are more efficient in hydrogen production and reveal a by a factor of 10-40 higher activity of H$_2$-cleavage (Frey 2002), but a lower substrate affinity than Ni-Fe H$_2$ases (Adams 1990; Frey 2002).

Fe-S cluster free H$_2$ases: Fe-S cluster free hydrogenases have been found in some methanogenic archaea (Figs. 1, 2). Originally, they have been considered to be metal free. Recently however, it has been established that there is a functional iron at the active site (Lyon *et al.* 2004).
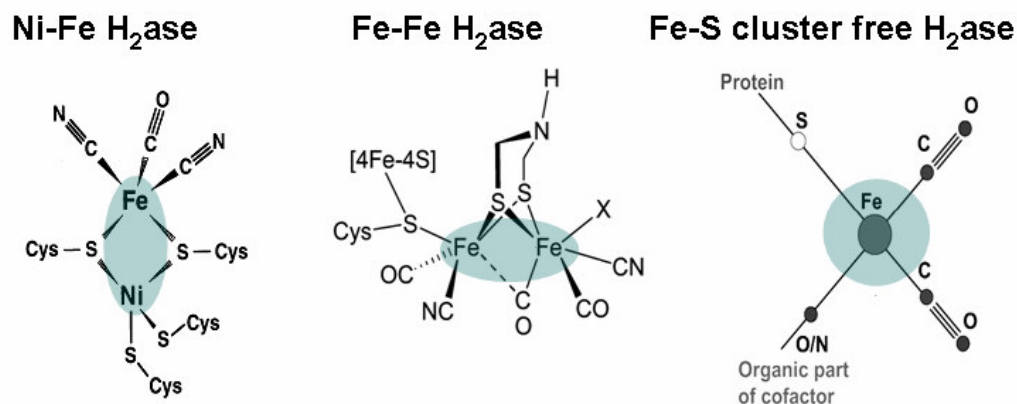

Figure 2: The three classes of hydrogenases as distinguished by their metal content in the active site (The model of the Ni-Fe H$_2$ase is taken from (Happe *et al.* 1997), the Fe-Fe H$_2$ase from (Schwartz *et al.* 2006), and the Fe-S cluster free H$_2$ase from (Korbas *et al.* 2006)).

Functional classification of hydrogenases

It has been found that numerous bacteria harbor distinct hydrogenases with different physiological roles associated with their respective localization in the cell (Ackrell *et al.* 1966). Three central functions of H_2ases can be distinguished (Vignais *et al.* 2001) (Fig. 3).

(1) Various organisms use hydrogen as an energy source by coupling H_2 oxidation to the reduction of electron acceptors such as carbon dioxide, sulfate, or sulfur. Hydrogen oxidation produces protons and electrons. Hydrogen consumption assays reveal specific activities of 100-800 U/mg in Ni-Fe hydrogenases and 10000-50000 U/mg in Fe-Fe hydrogenases (Albracht 1994). Uptake hydrogenases, such as periplasmic or membrane-bound hydrogenases, act as electron donors for electron transfer proteins (Fig. 3A) or the respiratory chain, respectively (Fig. 3B). By accumulating protons in one cell compartment, proton gradients are generated which subsequently are used for the synthesis of ATP.

(2) Production hydrogenases are usually found in obligate anaerobic bacteria. They catalyze the reduction of H^+ to dihydrogen (Fig. 3A) and function in reoxidation of reduced cofactors, such as NADPH, e. g., in archaea (Fig. 1); or serve to dispose excess reducing equivalents. Hydrogen production assays reveal a specific activity of 100-800 U/mg in Ni-Fe hydrogenases and 5000-10000 U/mg in Fe-Fe hydrogenases (Albracht 1994). Most hydrogenases are bidirectional and able to either cleave or produce hydrogen.

(3) Another interesting variant of hydrogenases are those which sense hydrogen. H_2-sensing is employed to regulate the expression of further hydrogenases in the cell. Such H_2 sensors are found in α and β proteobacteria (Lenz *et al.* 2001) (Fig. 1).
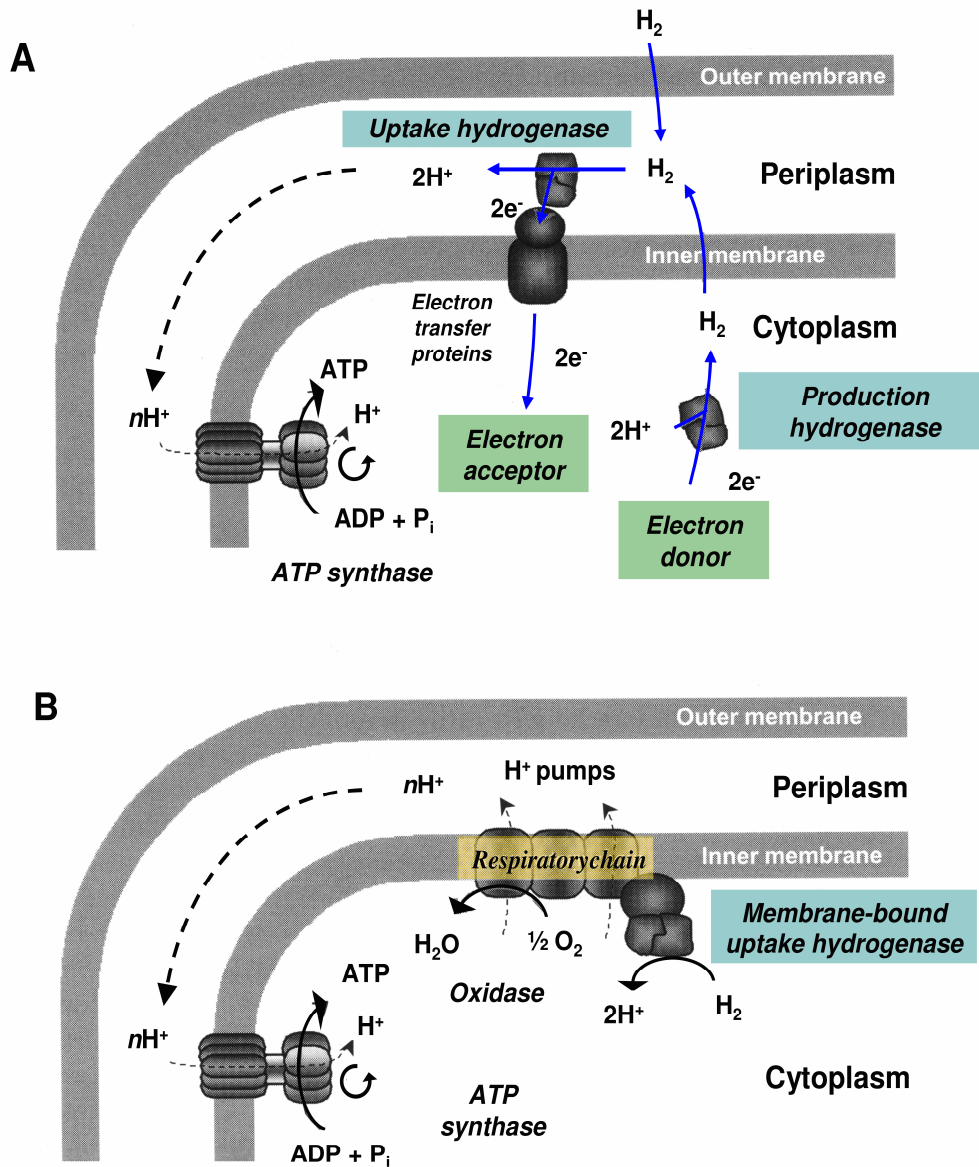
Figure 3: Energy conservation pathways in bacterial cells involving hydrogenases (adapted from (Cammack *et al.* 2001). **(A)** Simple mechanism (hydrogen cycling). Oxidation of H_2 by a periplasmic uptake hydrogenase and release of H^+ into the periplasm generates a proton gradient across the membrane. The proton gradient powers ATP production by the ATPase. **(B)** Mechanism where the membrane-bound uptake hydrogenase is linked to the respiratory chain.

Crystal structures of hydrogenases

Crystallographic structures have been reported for several hydrogenases, mainly of Ni-Fe H$_2$ases of the sulfate reducing bacteria of the genus *Desulfovibrio* (*D.*). Moreover, structures of a Ni-Fe-Se hydrogenase from *Desulfomicrobium* (*Dm.*) *baculatum* (Garcin *et al.* 1999), and of two Fe-Fe hydrogenases from *Clostridium* (*C.*) *pasteurianum* (Peters *et al.* 1998) and *D. desulfuricans* (Nicolet *et al.* 1999) have been reported. Table 1 summarizes available crystallographic structures.

Table 1: Available crystal structures of hydrogenases.

Class	Organism	Functional state	Resolution [Å]	Year	Reference	PDB code
Ni-Fe	*D. gigas*	unready	2.35	2005	(Volbeda *et al.* 2005)	1YQ9
	D. fructosovorans	unready	1.83	2005	(Volbeda *et al.* 2005)	1YQW
	D. fructosovorans	ready	2.1	2005	(Volbeda *et al.* 2005)	1YRQ
	D. fructosovorans	unready	1.04	2005	(Ogata *et al.* 2005)	1WUI
	D. vulgaris Miyazaki F	ready	1.4	2005	(Ogata *et al.* 2005)	1WUJ
	D. vulgaris Miyazaki F	active	1.4	2000	(Higuchi *et al.* 1999)	1H2R
	D. desulfuricans ATCC27774		1.8	2001	(Matias *et al.* 2001)	1E3D
Ni-Fe-Se	*Dm. baculatum*	active	2.2	1999	(Garcin *et al.* 1999)	1CC1
Fe-Fe	*C. pasteurianum*		1.8	1998	(Peters *et al.* 1998)	1FEH
	D. desulfuricans	mixed-reduced	1.6	1999	(Nicolet *et al.* 1999)	1HFE

Only references are given which correspond to the highest resolution structure. Right column: PDB entry number.

Ni-Fe hydrogenases

In a broad range of microbes (sulfate-reducing, nitrogen-fixing, methanogenic, and photosynthetic bacteria) Ni-Fe hydrogenases have been found (Fig. 1). The organisms live in diverse environments ranging from aerobic conditions at the top layer of aquatic ecosystems to the anaerobic sediment (Fig. 4). Seemingly, the Ni-Fe H$_2$ases are adapted to the O$_2$ content of the environment. Their tolerance against O$_2$ may vary according to the respective oxygen partial pressure (Vincent *et al.* 2005b).
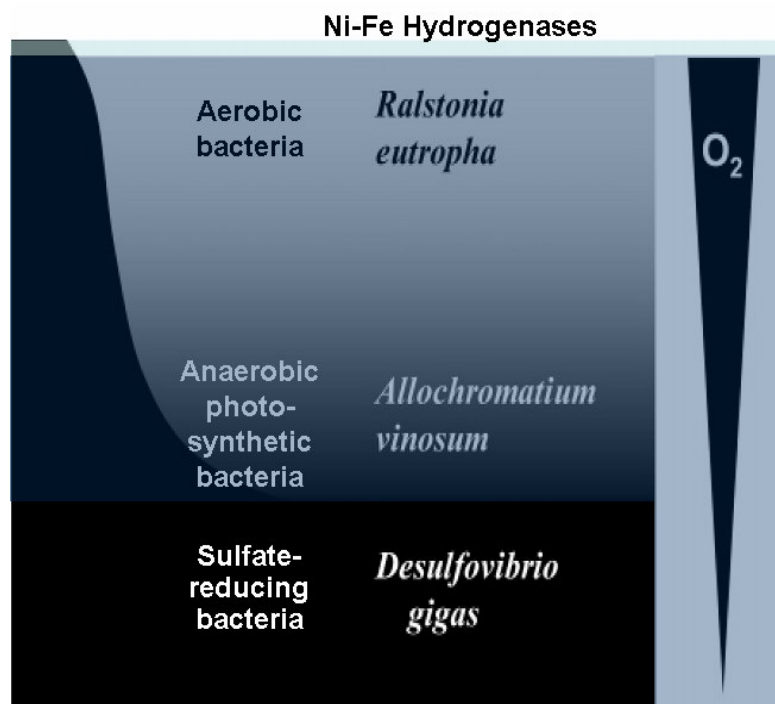
Figure 4: Predominant bacteria species in a pond (adapted from
(Cammack *et al.* 2001; Vincent *et al.* 2005b)).

Functional and spectroscopic investigations have revealed that certain Ni-Fe
hydrogenases show similar features. The main feature is the sensitivity against
inhibition by O_2 (Przybyla *et al.* 1992). These Ni-Fe hydrogenases have been termed
"standard" Ni-Fe hydrogenases. They include Ni-Fe hydrogenases from *D. gigas*, *D.
vulgaris*, *D. fructosovorans*, *Allochromatium* (*A.*) *vinosum*, and *Thiocapsa* (*T.*)
roseopercina (De Lacey *et al.* 2005). Crystal structures of several standard Ni-Fe
hydrogenases have provided detailed information on the molecular architecture of the
enzyme and in particular, on the organization of the catalytic site (see Table 1 and
Fig. 5) (Volbeda *et al.* 1995; Higuchi *et al.* 1997; Ogata *et al.* 2005; Volbeda *et al.*
2005). The molecular weight of standard Ni-Fe hydrogenases is about 100 kDa. They
are composed of a large and a small subunit. The large subunit carries the Ni-Fe site
which is deeply buried in the protein. The small subunit accommodates three
iron-sulfur clusters, a proximal [4Fe-4S(cys)$_4$], a medial [3Fe-4S(cys)$_3$] and a
[4Fe4S(cys)$_3$(his)] cluster in the distal position (Cammack *et al.* 2001). The Fe-S
clusters are arranged in a row from the center to the surface of the protein (see also
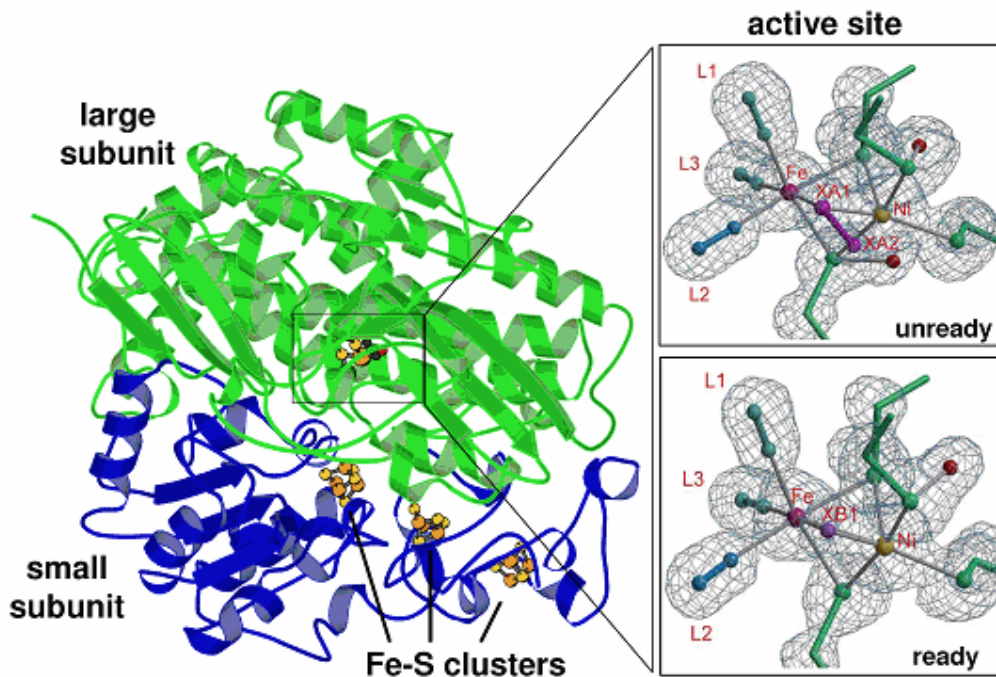Fig. 6) (Volbeda *et al.* 1995; Higuchi *et al.* 1997).

Figure 5: Crystal structure of the heterodimeric Ni-Fe H$_2$ase from *D. vulgaris* Miyazaki F and electron density map of the active site (Ogata *et al.* 2005). **Left:** The large subunit (top, green) contains the Ni-Fe active site and the small subunit (bottom, blue) three iron-sulfur clusters. **Right:** Electron density distribution around the Ni-Fe active site of *D. vulgaris* Miyazaki F with a ball-and-stick model of the unready and ready states adapted from (Ogata *et al.* 2005). The non-protein bridging ligand is depicted in magenta and the diatomic ligands (CN and CO) at the Fe atom are marked L1 to L3.

The Ni-Fe complex is linked to the protein by thiols provided by cysteine residues (Albracht 1994; Cammack *et al.* 2001). The Ni atom is coordinated by four thiol groups; two of these are bridging ligands that also coordinate the Fe (Figs. 2, 5). The Fe atom is further ligated by three inorganic diatomic ligands identified by FTIR spectroscopy as one CO and two CN$^-$ in *A. vinosum* (Happe *et al.* 1997) and *D. gigas* (De Lacey *et al.* 1997). In the inactive as-isolated, oxidized enzyme, a third non-protein bridging ligand between the nickel and the iron atom has been detected (Fig. 5). Recent crystallographic data of *D. fructovorans* hydrogenase suggest a peroxidic group in the unready and a hydroxide ligand (OH$^-$) in the ready form (Volbeda *et al.* 2005) (for characterization of the unready and ready form of the enzyme see also the following section). The oxygen species is related to the activation process. Under reducing conditions, the disappearance of the bridging oxygen species has been observed in crystals of Ni-Fe hydrogenases (Garcin *et al.* 1999; Higuchi *et al.* 1999). EPR studies (Carepo *et al.* 2002; Foerster *et al.* 2003), corroborated by density functional theory (DFT) calculations, suggested that the oxygen-species is exchanged

by a bridging hydride ($Ni^{III} - H^- - Fe^{II}$) (Amara *et al.* 1999; Stein *et al.* 2001a; Brecht *et al.* 2003). The bridging hydride has not been detectable in crystallographic electron density maps even at 1.4 Å resolution (Higuchi *et al.* 1999), as expected.
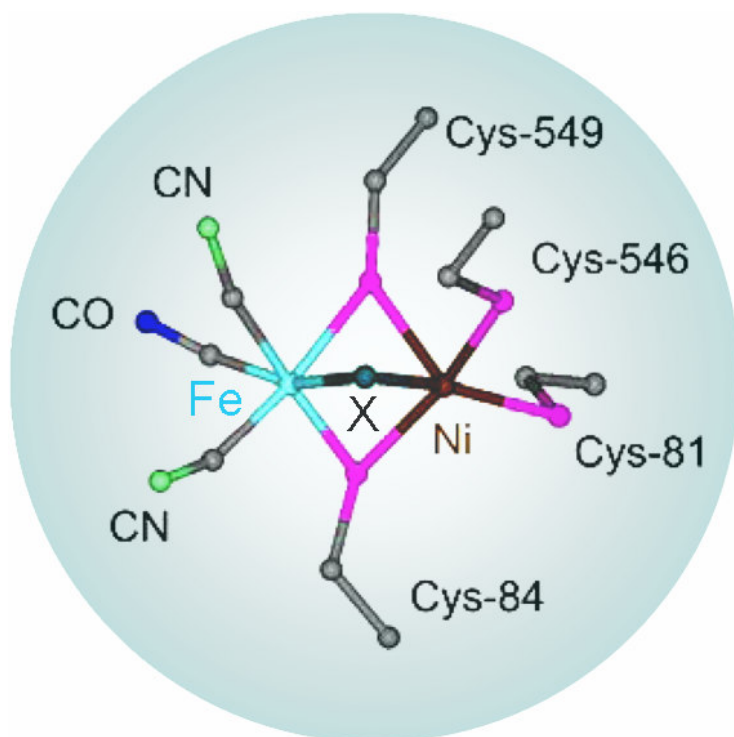

Figure 6: Three-dimensional structure constructed on the basis of crystallographic data and DFT calculations of the Ni-Fe active site of standard hydrogenases (adapted from (Van Gastel *et al.* 2006)). The Ni atom is coordinated by four thiol groups provided by cysteine residues and a bridging ligand (X). This ligand is attributed in the oxidized enzyme to a peroxidic group in the unready and a hydroxide ligand in the ready form (Volbeda *et al.* 2005) and to a bridging hydride in the reduced enzyme. The Ni atom is in a distorted square-pyramidal conformation with a vacant sixth ligand site. The Fe atom is six-coordinated by the three bridging ligands and three terminal non-protein ligands, one CO and two CN. The ligands at the Fe are arranged in a distorted octahedral conformation.

Details of the three-dimensional structure of the Ni-Fe active site of standard Ni-Fe hydrogenases are shown in Fig. 6 (Stein *et al.* 2001b). The Ni atom is five-coordinated in a distorted square-pyramidal conformation with a vacant sixth binding site. The Fe atom has six ligands in the presence of the hydride in a distorted octahedral conformation.

The active site of Ni-Fe hydrogenases, where the reaction with hydrogen takes place (see Eq. 1) is deeply buried in the center of the protein. For the H_2 uptake reaction, the hydrogen molecule has to reach the bimetallic center. H_2 cleavage is believed to occur heterolytically. In the first step, a hydride (H^-) and a proton (H^+) are formed. Then, presumably the two electrons of the H^- are extracted, resulting in the formation of another proton. The electrons are transferred to the Fe-S clusters and then to exogenous electron acceptors. For hydrogen production the sequence of events is reversed. A scheme of the pathways of reactant and electron flows is shown in Fig. 7.
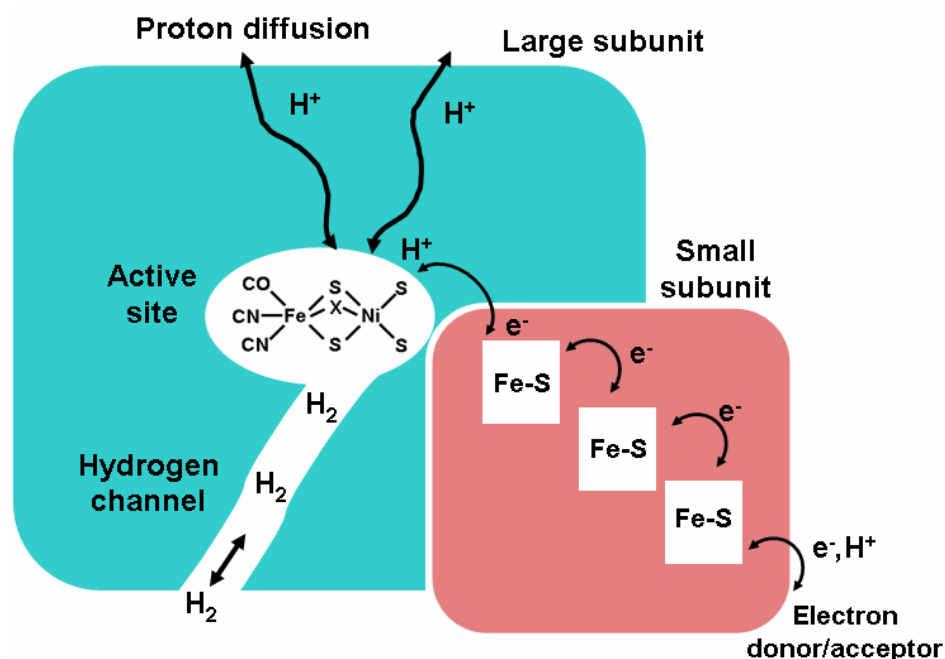

Figure 7: A scheme of the pathways of reactant and electron flows from the Ni site to the protein surface.

Crystallographic analysis of Xenon-gas treated hydrogenase revealed the existence of a net of hydrophobic channels within the protein (Montet *et al.* 1997) (Fig. 8). Molecular dynamics simulations of Xe and hydrogen diffusion processes suggested that these channels serve as a gas access to the active site. One end of the channel network points to the vacant coordination site of the Ni (Montet *et al.* 1997). Numerous other ends lead out to the external medium (Montet *et al.* 1997). Several routes for proton movements in Ni-Fe-hydrogenases have been proposed (Garcin *et al.* 1999), but these pathways have to be confirmed by site-directed mutagenesis studies (Cammack *et al.* 2001).

Figure 8: Gas accessibility to the Ni-Fe active site (adapted from (Montet *et al.* 1997)). Blue spheres indicate xenon atoms in the crystal structure of *D. fructosovorans* Ni-Fe H$_2$ase. Twelve internal Xe atoms were found. The blue grid shows an accessibility map of the enzyme, indicating conserved hydrophobic cavities and channels. These channels may function in providing H$_2$ access to the deeply buried active site.
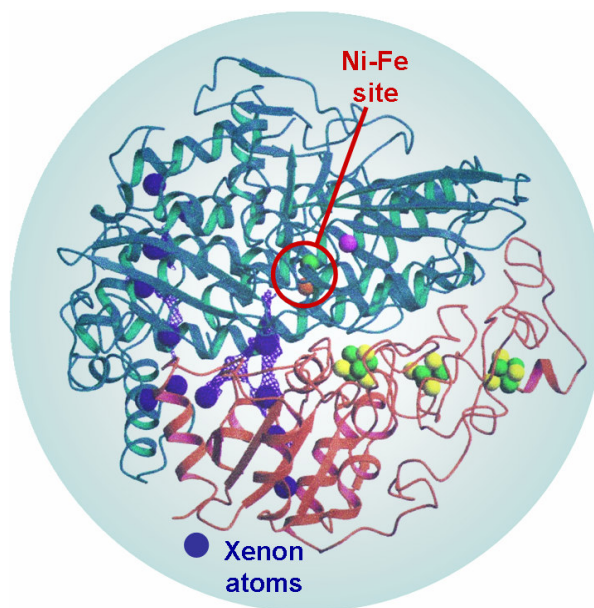
Redox-titrations in combination with spectroscopic studies show that the iron-sulfur clusters are involved in the redox processes (Frey 1999). The Fe-S clusters are arranged almost in a linear row with roughly equal spacing by ~ 10Å between them (Figs. 7-9), thereby forming an electron transfer chain from the Ni site to the protein surface (Volbeda *et al.* 1995).
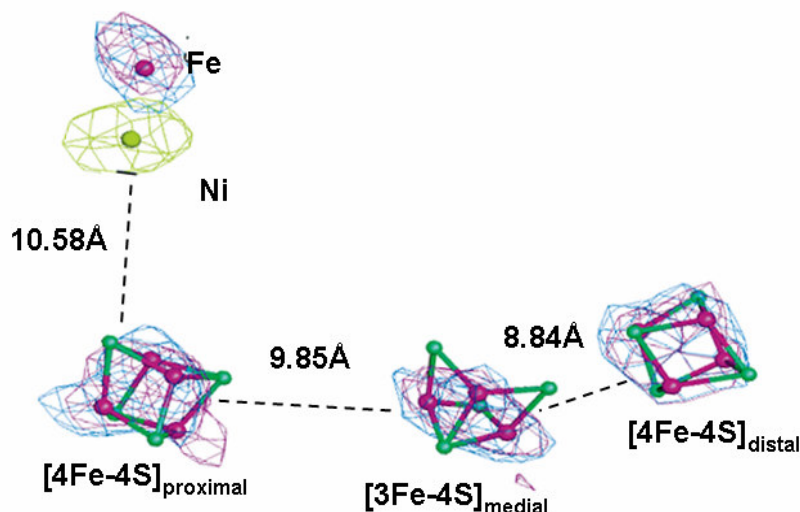

Figure 9: Cofactor arrangement and electron transfer chain in the Ni-Fe hydrogenase of *D. vulgaris* Miyazaki F (Higuchi *et al.* 1997). The three Fe-S clusters have been identified as [4Fe-4S] (proximal), [3Fe-4S] (medial), and [4Fe-4S] (distal).

Redox states of the active site detected by EPR and FTIR

Standard Ni-Fe hydrogenases show a complex redox chemistry. Several intermediates in the catalytic cycle have been described which differ with respect to oxidation state and coordination of the Ni atom (Cammack *et al.* 2001). Samples of standard Ni-Fe hydrogenases purified under aerobic conditions are catalytically inactive. They can be activated under reducing conditions.
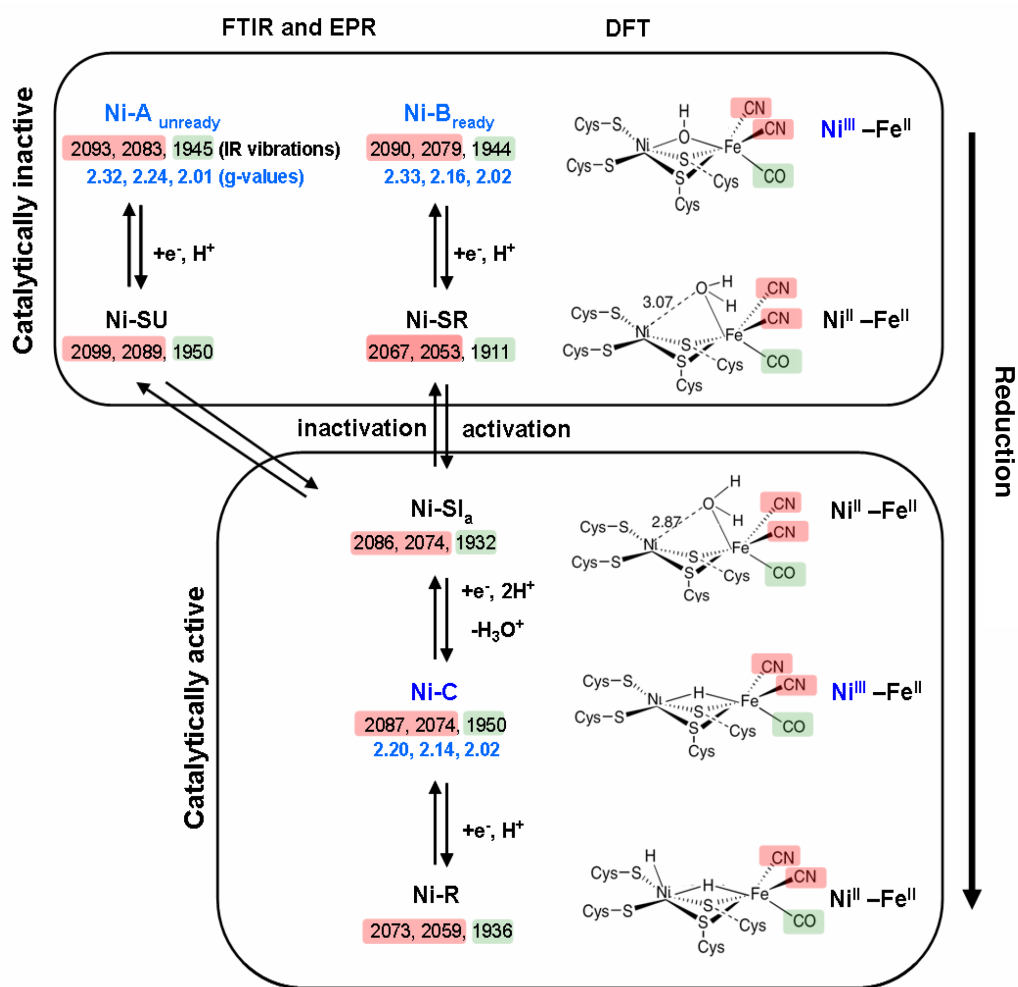

Figure 10: The redox states of the active site (adapted from (Stein *et al.* 2002)). Right: One proposed model of catalytic cycles with structures which are based on DFT geometry optimizations from Ni-B to Ni-R (adapted from (Stein *et al.* 2004). EPR-detectable paramagnetic states (Ni^{III}) are assigned by their respective g-values (blue). The diamagnetic states (Ni^{II}) characterized by FTIR are given in black. During reduction, the Fe atom remains in the Fe^{II} oxidation state. In all states the characteristic IR stretching frequencies (in cm^{-1}) of the two CN^- (marked in red) and one CO (marked in green) ligands are shown. DFT calculations predict a geometrical change for the transition from Ni–SR to Ni–SI$_a$ (bond distances (Ni-O) are given in Å (Stein *et al.* 2004)).

Figure 10 shows a summary of the redox states of the active site of standard Ni-Fe H_2ases detected on the basis of EPR and FTIR spectroscopy. The respective structural proposals which are based on DFT calculations are shown on the right (Stein *et al.* 2004) (for further models of the catalytic cycle with varying intermediate states see (Pardo *et al.* 2006)).

By EPR spectroscopy changes in the electronic configuration of the Ni atom of the active site can be monitored. Three typical signals have been characterized. The inactive aerobically isolated samples of standard Ni-Fe hydrogenases usually show a mixture of two EPR signals, namely the Ni-A and Ni-B signals (De Lacey *et al.* 1997). These signals are due to two different paramagnetic Ni^{III} species (Figs. 10, 11A). They differ in the time course of their disappearance during activation and with respect to the coordination of the Ni site. The Ni-B (ready) form is activated within minutes under H_2 atmosphere, whereas the Ni-A form (unready) requires several hours for activation (Fernandez *et al.* 1985). The third EPR signal due to Ni^{III} (Ni-C) appears gradually upon reductive activation. The Ni-C signal is attributed to a catalytically active state of the enzyme (Teixeira *et al.* 1985) with a ($Ni^{III} - H^{-} - Fe^{II}$) conformation (Figs. 10, 11A). The dependence of the magnitude of the Ni-B and Ni-C EPR signals on the redox-potential (De Lacey *et al.* 2005) is shown in Fig. 10B.
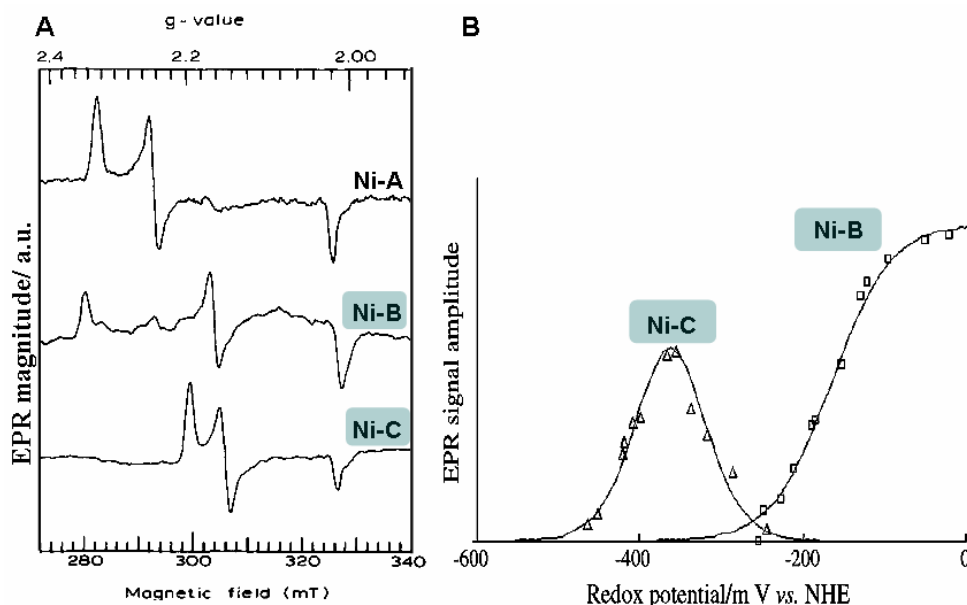

Figure 11: Typical EPR spectra of *D. gigas* hydrogenase. **(A)** The Ni-A, Ni-B, and Ni-C signals state are shown, attributed to Ni^{III} (adapted from (Cammack *et al.* 1987). **(B)** EPR-monitored redox titrations of the active site (De Lacey *et al.* 2005). The Ni-C signal is visible only in a narrow range of redox potentials.

FTIR studies of Ni-Fe hydrogenase have revealed three absorption bands in the 2100-1900 cm^{-1} spectral region (Fig. 12). These bands have been identified (Happe *et al.* 1997), on the basis of isotopic labeling of the enzyme, as two CN^{-} and one CO coordinated to the iron atom of the active site (see also Fig. 6). Frequency shifts of these bands in the catalytic cycle reveal changes in the electron density at the Fe atom (De Lacey *et al.* 2005). By FTIR not only the paramagnetic states, but all states are visible.
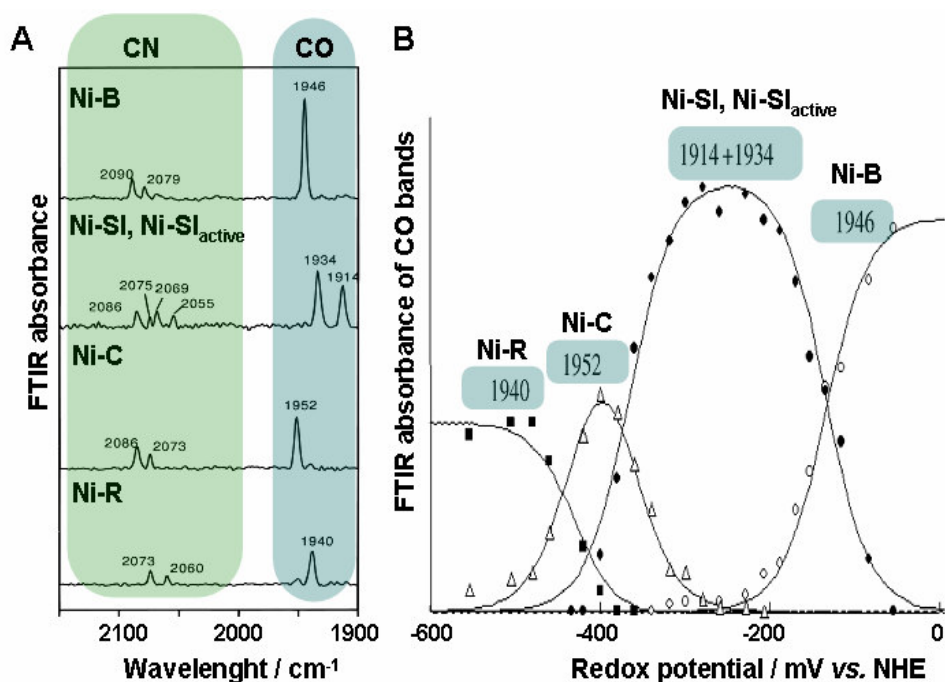

Figure 12: Typical FTIR spectra of *D. gigas* hydrogenase (adapted from (De Lacey *et al.* 1997; De Lacey *et al.* 2005). **(A)** FTIR spectra of different redox states of the active site with their respective band positions. Slight variations in band positions in comparison to other standard Ni-Fe hydrogenases have been observed. The spectral region of the CN bands is highlighted in green, the region of the CO bands in blue. **(B)** FTIR-monitored redox titrations of the active site. The integrated absorption intensity of the respective CO bands has been used as a measure for state population (De Lacey *et al.* 2005).

The Ni-Fe hydrogenases of *Ralstonia eutropha*

Ralstonia eutropha (*R. eutropha*, formerly called *Alcaligenes eutrophus*) (Fig. 13) is a chemolitho-autotrophic proteobacterium and belongs to the knallgas bacteria (Cammack *et al.* 2001; Lenz *et al.* 2002). It is able to use hydrogen as the sole energy source (Friedrich *et al.* 2005). *R. eutropha* is found in the top layer ofaquatic ecosystems where the water is oxygen rich (compare Fig. 4).

Accordingly, the Ni-Fe hydrogenases of *R. eutropha* should be functional under aerobic conditions. Indeed, already early investigations on the enzymes revealed their O_2-tolerance (Adams *et al.* 1981). This behavior is in contrast to standard Ni-Fe hydrogenases which are inhibited already by small amounts of O_2 in the medium.

Figure 13: Cells of the proteobacterium *R. eutropha* which possess three different Ni-Fe hydrogenases, namely the soluble H_2ase (SH), the regulatory H_2ase (RH), and the membrane-bound H_2ase (MBH).

R. eutropha possesses three distinct Ni-Fe hydrogenases (Lenz *et al.* 1998) which play different physiological roles in the cell (Lenz *et al.* 2001). A complex maturation process is required for the assembly of the enzymes and the incorporation of the Ni-Fe site. This process is assisted by auxiliary proteins (for a review see (Burgdorf *et al.* 2005a). Two energy-converting Ni-Fe hydrogenases, a membrane-bound enzyme (MBH), and a soluble hydrogenase (SH) have been described. The third protein, the so-called regulatory hydrogenase (RH), functions as a H_2-sensor. Because of their oxygen tolerance, these H_2ases are potentially interesting for biotechnological applications. No crystal structure of these enzymes is available.

The three hydrogenases of *R. eutropha* are the subject of this thesis. The studies presented in this work would not have been possible without the strong collaborative input of the group of Prof. Bärbel Friedrich (Microbiology at Humboldt University, Berlin, Germany). This group has provided the protein samples (more than 80 individual H_2ase samples of high protein concentration (~1 mM)) for our spectroscopic measurements.

The soluble hydrogenase (SH)

The soluble hydrogenase (SH) of *R. eutropha* resides in the cytoplasm. It belongs to the group of multimeric, so-called bidirectional hydrogenases (Vignais *et al.* 2001). The SH shows extensive similarities to complex I (NADH: ubiquinone oxireductase) (Albracht *et al.* 2000), including amino acid sequence similarities, a related pattern of Fe-S clusters, and the possible presence of two FMN groups (Albracht *et al.* 2003) (Fig. 14).
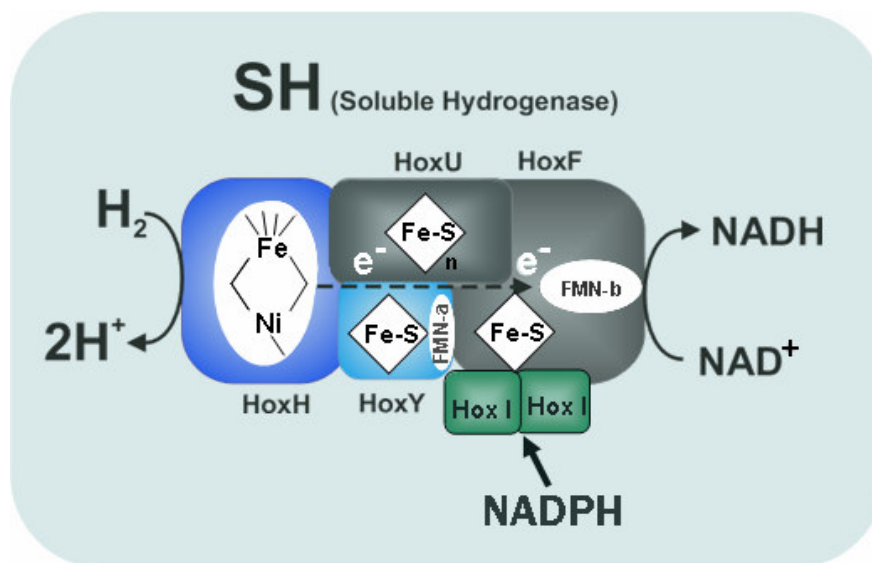
Figure 14: Organization of the soluble H_2ase (SH). The hydrogenase heterodimer (blue) is encoded by the genes HoxH and HoxY. The large subunit HoxH carries the Ni-Fe site. The small HoxY subunit is a truncated version of the small subunit of the standard Ni-Fe hydrogenases. It presumably carries only one [4Fe-4S] cluster (Burgdorf *et al.* 2005c). Additionally one flavin mononucleotide molecule (FMN-a) in HoxY has been proposed to be present which may be essential for H_2 turnover (Van der Linden *et al.* 2004). The hydrogenase module is attached to the diaphorase module (NADH dehydrogenase) (grey) which consists of a small subunit (HoxU) and a large subunit (HoxF). The HoxU subunit likely carries one [4Fe-4S] cluster and one [2Fe-2S] cluster. The HoxF subunit harbors one further [4Fe-4S] cluster and one FMN (FMN-b) molecule. HoxF furthermore provides the NAD^+-binding site (Tran-Betcke *et al.* 1990). The electrons derived from H_2 cleavage presumably are transferred from the Ni-Fe site via the Fe-S clusters and FMN-b to NAD^+ (Erkens *et al.* 1996). Two HoxI subunits (in green) probably are linked to the HoxF and HoxY subunit, providing a NADPH binding site. It has been observed that only enzymes which contain the HoxI I subunits can be activated by NADPH. For more details see (Burgdorf *et al.* 2005c).

In the SH, the oxidation of H_2 is directly coupled to the reduction of NAD^+. Thereby reducing equivalents for biosynthesis are provided. The SH can catalyze H_2 production, although at a low rate (Schneider *et al.* 1976). The SH is a heterohexamer (Burgdorf *et al.* 2005c) (Fig. 14). Its six subunits are arranged in two functionally distinct modules, the hydrogenase and the diaphorase, linked to a monodimeric unit $(HoxI)_2$. The large subunit of the hydrogenase module (HoxH) contains the Ni-Fe active site. The small subunit (HoxY) and the diaphorase module harbor the Fe-S clusters and FMN (Fig. 14). Biochemical and spectroscopic investigations have revealed several unusual features of the SH. Further details can be found in the introduction sections of **Chapters 2 and 3**.

In this thesis, various wild-type and mutant SH preparations in several redox states were studied to obtain information on structural features of the Ni-Fe cofactor in the native SH, to unravel the mechanism of reductive activation, and to learn about the catalytic mechanism. One goal was to gain information on the reasons for the oxygen tolerance.

The regulatory hydrogenase (RH)

The regulatory hydrogenase (RH) of *R. eutropha* is involved in hydrogen sensing. It resides in the cytoplasm. The RH is a multisubunit system, consisting of a dimeric heterodimer (HoxBC)$_2$ which is firmly linked to a histidine protein kinase homotetramer (HoxJ) (Bernhard *et al.* 2001; Lenz *et al.* 2002; Buhrke *et al.* 2004) (Fig. 15).
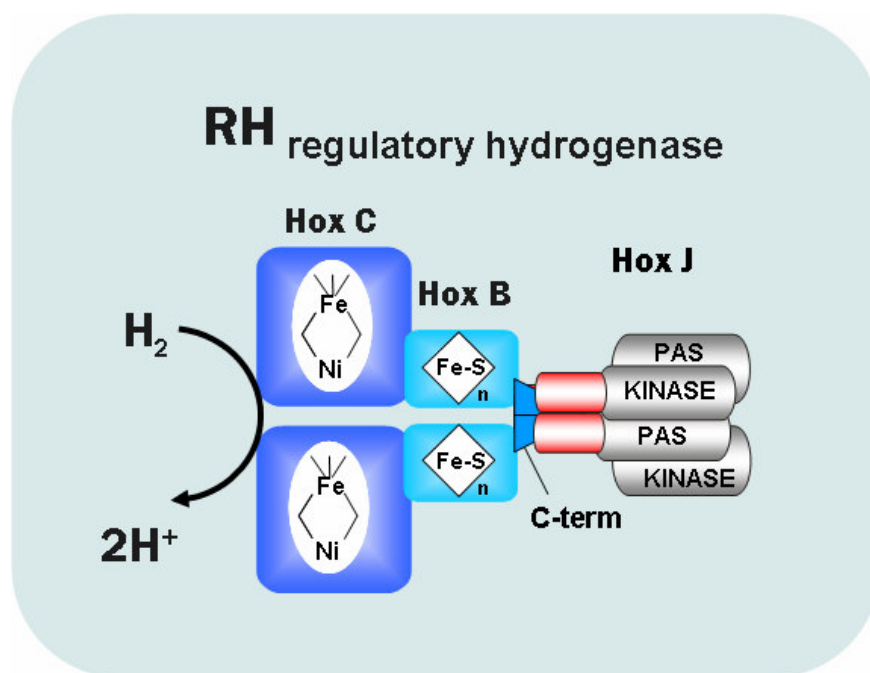

Figure 15: Organization of the regulatory H$_2$ase (RH) from *R. eutropha* (adapted from (Burgdorf *et al.* 2005a)). The RH has a molecular weight of 380 kDa. This complex is formed by a dimeric heterodimer (HoxBC)$_2$. Each of the large HoxC subunits of the double dimer contain one Ni-Fe site. The small subunits (HoxB) comprise the Fe-S clusters. The 55-amino-acid C-terminal extension (Kleihues *et al.* 2000) is required for the ((HoxBC)$_2$) dimer formation, and for the formation of the complex with the histidine protein kinase tetramer (HoxJ). HoxJ is divided into a PAS domain and the kinase module. The PAS domain is involved in signal transduction (see Fig.16).

Interaction of the RH with H_2 initiates a complex signal transduction cascade (Lenz *et al.* 1998), regulating the gene expression of the energy-converting hydrogenases, SH and MBH (Fig. 16).
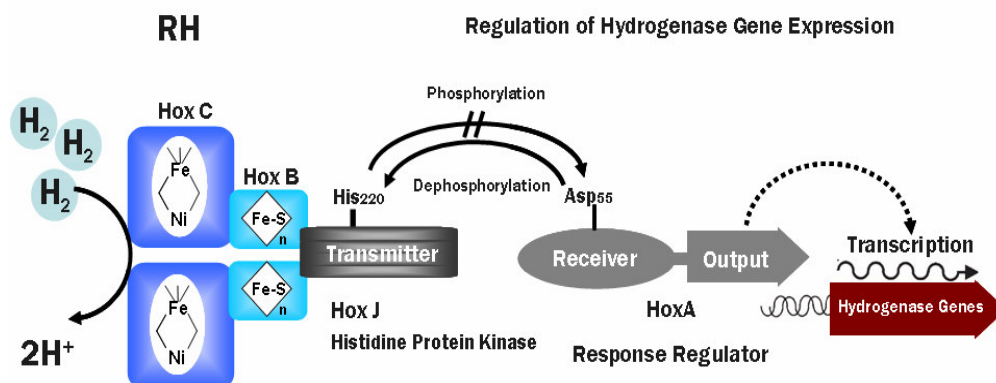

Figure 16: A model of the H_2 -sensing signal transduction chain of the RH (adapted from (Burgdorf *et al.* 2005a)). The binding of H_2 to the active site of the HoxC subunits initiates a signal transduction cascade leading to the expression of hydrogenases genes of SH and MBH. The His_{220} of HoxJ interacts via phosphorylation/ dephosphorylation with Asp_{55} of the response regulator HoxA. In the presence of hydrogen, either phosphorylation of HoxA is inhibited or dephosphorylation of HoxA is initiated. HoxA is active in its non-phophorylated form and inactive after HoxJ-mediated phosphorylation (Burgdorf *et al.* 2005a).

Like the two other hydrogenases of *R. eutropha*, the RH is insensitive to inhibition by oxygen. Apparently, the RH is always ready to react with hydrogen; reductive activation is not required. This has been concluded from the absence of a lag phase at the onset of hydrogen cleavage (Pierik *et al.* 1998b) (Fig. 17). This feature is a prerequisite for the sensor function of the RH because the protein should be "on alert" to receive the signal. However, the H_2-oxidizing activity of about 0.8 U/mg of the RH is 1-2 orders of magnitude lower than the activity, e. g., of the SH (Pierik *et al.* 1998b).
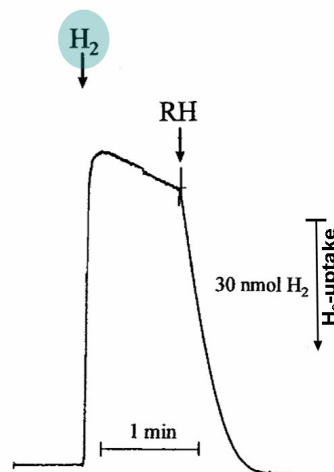

Figure 17: Hydrogen uptake activity of the RH (adapted from (Pierik *et al.* 1998b)). The reaction was started by the addition of RH to a solution of air-saturated buffer solution with 25 mM benzyl viologen. No lag phase is observable.

The RH has been previously investigated by EPR (Pierik *et al.* 1998a), FTIR (Bernhard *et al.* 2001), and XAS (Haumann *et al.* 2003). In this thesis two studies of distinct RH constructs (the double dimeric form (HoxBC)$_2$, the monodimeric form (HoxBC), and the isolated HoxC subunit) are presented (**Chapters 4, 5**). The Ni-Fe site and the Fe-S clusters have been characterized. One question was how electron transfer within the RH functions.

The membrane-bound hydrogenase (MBH)

The membrane-bound (MBH) of *R. eutropha* belongs to the uptake Ni-Fe hydrogenases found in bacteria and archaea (Vignais *et al.* 2004) (see Fig. 1). The MBH is a heterodimer with a large subunit (HoxG) and a small subunit (HoxK) (Lenz *et al.* 2005) (Fig. 18). HoxG harbors the Ni-Fe active site. The amino acid sequence of HoxK predicts the coordination of three Fe-S clusters (Bernhard *et al.* 1996).
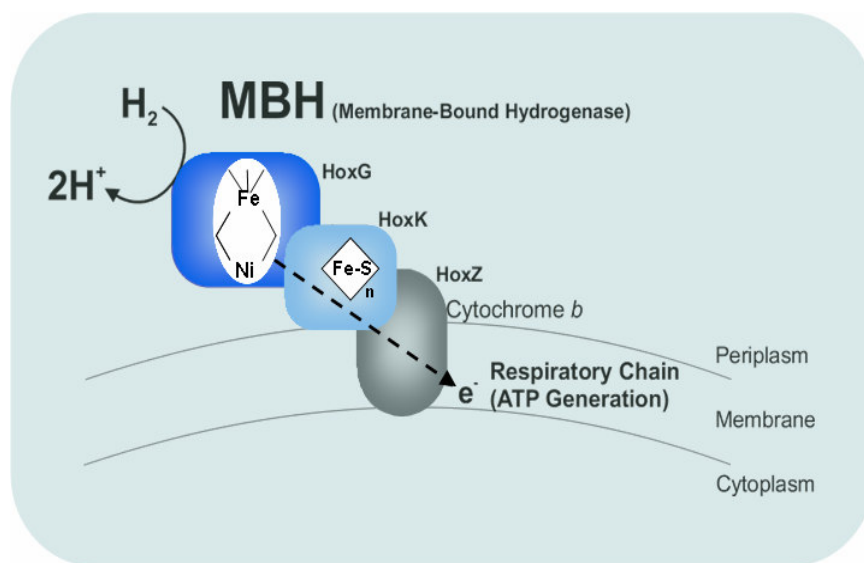

Figure 18: Organization of the membrane-bound H$_2$ase (MBH) from *R. eutropha* (adapted from (Burgdorf *et al.* 2005a)). The MBH is a heterodimer, which is linked to Cyt-b. The Cyt-b serves as a primary electron acceptor and is coupled to the respiratory chain (see also Fig. 3). The large HoxG subunit (67.1 kDa) contains the Ni-Fe active site and the small HoxK subunit (34.6 kDa) Fe-S clusters.

The MBH faces the periplasm. The transport of the fully assembled MBH across the membrane from the cytoplasm to the periplasm is catalyzed by the twin-arginine-translocations (TAT) system (Burgdorf *et al.* 2005a). The MBH is linked to cytochrome-b (Cyt-b) which is inserted in the cytoplasmic membrane. The Cyt-b serves a primary electron acceptor of the MBH.

The MBH is able to maintain partial hydrogen oxidation activity in the presence of oxygen (Vincent *et al.* 2005a; Vincent *et al.* 2005b) (Fig. 19). This enzyme recovers rapidly after exposure to O_2. In contrast to the oxygen-tolerant MBH of *R. eutropha*, the H_2 uptake activity of the *A. vinosum* H_2ase is completely abolished after addition of small amounts of O_2 (partial pressure of O_2 of 5 mbar). Even after removal of oxygen, this enzyme shows no recovery of the activity.
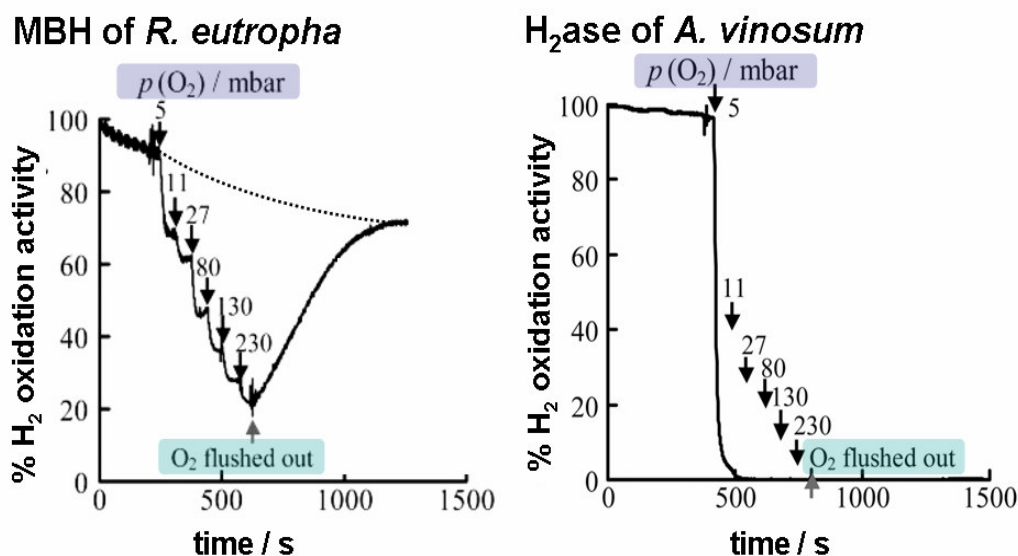

Figure 19: The effect of O_2 partial pressure (pO_2) on the H_2 oxidation activity of electrode-adsorbed films of the membrane-bound H_2ases of *R. eutropha* and *A. vinosum* (adapted from (Vincent *et al.* 2005a)). The H_2 oxidation activity of the MBH of *R. eutropha* is diminished after addition of oxygen (stepwise increasing of the partial O_2 pressure). After removal of O_2, the MBH of *R. eutropha* recovers completely (taking into account the gradual loss of enzyme from the electrode). In the *A. vinosum* H_2ase the activity is abolished even with a pO_2 of 5 mbar. No recovery of the enzyme is observable after elimination of the oxygen.

In addition to the oxygen-tolerance of the enzyme, the activity of the MBH also is unaffected by CO (Vincent *et al.* 2005a). These features make the MBH promising for biotechnologically applications, e. g., for the use as electro-catalyst in fuel cell arrangements. In this thesis the active Ni-Fe site and the Fe-S clusters of the MBH are characterized for the first time by XAS (**Chapter 6**). The objective was to achieve information on the atomic structure of the cofactors.

X-ray absorption spectroscopy on biological samples (BioXAS)

X-ray absorption spectroscopy (XAS) has developed into an important tool in metalloprotein research. The technique is neither restricted to specific elements nor are specific oxidation or spin states required. Furthermore, crystalline samples are not needed, a crucial advantage because crystals are available only for a minor fraction of metalloenzymes. Therefore, XAS is applicable to a broad range of biological samples (BioXAS). Analysis of XAS spectra provides information on the local structure of metal sites and the metal oxidation state. The various states occurring during catalysis can be characterized by this technique. In particular the metal-ligand distances are determined by XAS at an precision (± 0.02 Å) largely exceeding the one normally obtained by X-ray crystallography of proteins.

Today X-rays from a high intensity synchrotron radiation source usually are employed for BioXAS. The XAS method is based on the photoelectric effect (Fig. 20).
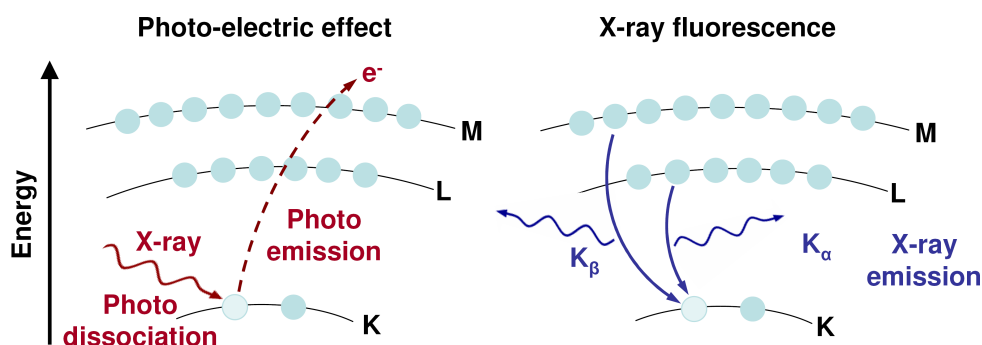

Figure 20: Scheme of the photoelectric process and the resulting X-ray fluorescence. Absorption of an X-ray photon occurs when its energy is tuned to the binding energy of a core level electron. The core electron (e. g. a K-shell electron), is excited into the continuum. An electron from a higher level drops into the core hole, accompanied by the emission of an X-ray fluorescence photon.

The absorption of an X-ray photon by a metal atom (absorber) promotes the excitation of a core-level electron (1s) into the continuum or to bound unoccupied levels (Figs. 20, 21). This leaves the atom in an excited state with an empty electronic level, the core-hole. Subsequently the excited state relaxes back to the ground state by filling the core-hole with a higher-level core-electron under emission of X-ray fluorescence.
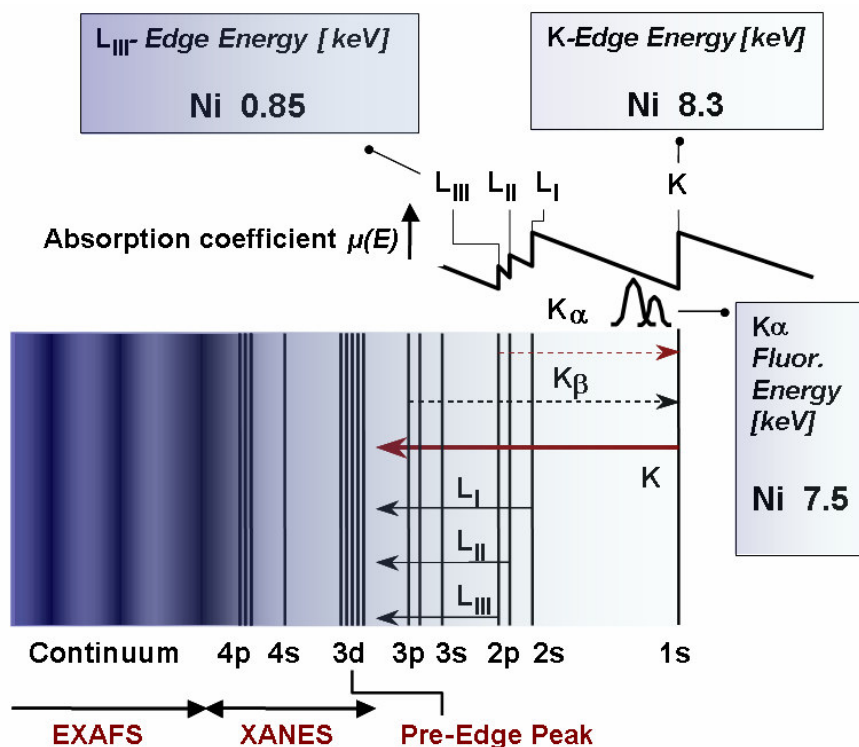
Figure 21: Schematic electronic energy level diagram. During an energy scan (see the schematic X-ray absorption spectrum), no absorption occurs until the photon reaches an energy above the Fermi energy. At higher energies, an 1s electron is excited into bound states (3d, 4p) or into the continuum, resulting in the K-edge absorption spectrum. X-ray excitation of 2p or 2s electrons gives rise to the L_{III}, L_{II}, and L_{I} absorption edges. The given energy values refer to Ni.

When the energy of the incident X-ray photons is sufficient to cause excitation of an 1s core electron of the absorbing atom, a sharp rise in the absorption, the K-edge, is observed (Figs. 21, 24). The energy position of the K-edge corresponds to the binding energy of an 1s electron and is therefore related to the atomic number of the absorber.

XAS determines the energy dependence of the X-ray absorption coefficient $\mu(E)$ at and above the absorption edge of a chosen element. $\mu(E)$ can be calculated by two methods. In the transmission mode the absorption is calculated from the ration of the transmitted photon flux I behind the sample of the thickness x and the incident X-ray flux I_0 according to Eq. 2 (Lambert-Beer law) (Figs. 22).

$$\mu(E)x = ln(I / I_0) \tag{2}$$

For highly diluted samples, e. g., protein samples (concentrations of ≤ 1 mM of metal) fluorescence detected absorption spectra are measured. The fluorescence intensity (I_f) is proportional to the absorption coefficient according to Eq. 3.

$$\mu(E) \sim I_f / I_0 \qquad\qquad\qquad \textbf{(3)}$$

For fluorescence measurements an energy-resolving fluorescence detector, usually solid-state detectors with Ge or Si crystals as X-ray absorbers, is used. A scheme of the experimental setup is shown in Fig. 24.

The XAS studies in this work have been carried out at the Ni and Fe K-edges. An element-specific XAS spectrum is obtained by scanning the respective energy range. For samples containing more than one atom of the specific element per protein, an average spectrum of all atoms is obtained (Fig. 22). The XAS spectrum can be divided into three main regions reflecting different physical processes, namely the pre-edge and main edge regions (**X**-ray **A**bsorption **N**ear **E**dge **S**tructure, **XANES**) and the **E**xtended **X**-ray **A**bsorption **F**ine **S**tructure (**EXAFS**) at energies well above the edge.
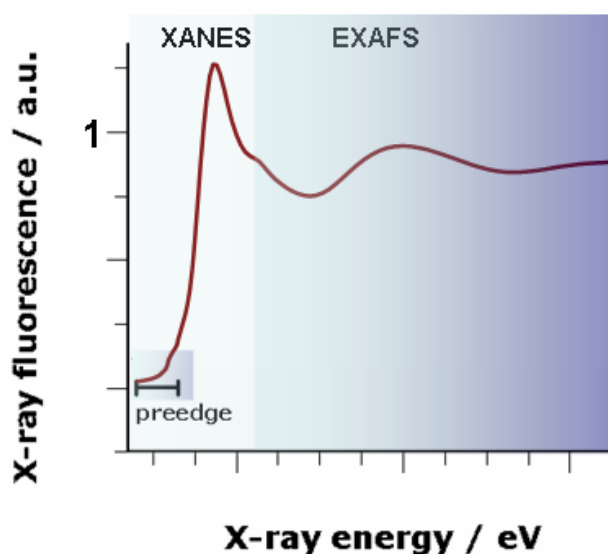

Figure 22: Schematic XAS spectrum. The three different regions of the spectrum are indicated (Pre-edge, XANES, and EXAFS regions).

The position on the energy scale and the shape of the edge provide information on the metal oxidation state, on the number and geometry of metal ligands, and on their chemical nature, respectively. The pre-edge peak is attributed to dipole-forbidden $1s \rightarrow 3d$ transitions. This feature is indicative, e. g., of the symmetry at the metal atom. Comparably large pre-edge peak features are observed, e. g. for planar geometries and metal=oxo motifs. In the XANES region, transitions of core electrons to bound unoccupied levels ($1s \rightarrow 4p$) occur. Qualitative evaluation of the XANES region often is based on comparison with spectra of model compounds which mimic relevant features of the metal site in the protein. In recent years *ab initio* simulation of the XANES region for its quantitative evaluation has become feasible (Rehr *et al.* 2001; Benfatto *et al.* 2003).

The EXAFS region of the spectrum starts at about 40 eV above the edge. The photoelectron is excited into the continuum and can be represented by an outgoing electron wave. Accordingly, the EXAFS region of the spectrum is described using scattering theory. In this framework, the EXAFS oscillations result from interference of outgoing and electron waves that are backscattered at neighboring atoms of the absorber causing constructive or destructive interference. The amplitude and frequency of a resulting modulation of the X-ray absorption depends on the chemical nature of the neighboring atoms and their distance to the absorber.

Direct scattering (single scattering path) or multiple scattering by a path involving more than one backscattering atom is observed (Fig. 23). Particular strong multiple-scattering effects are observed, e. g., for the linear arrangement of the backscatterers (metal CN or metal-CO bonds) and for aromatic ligands (Histidine).

Figure 23: Scheme of single and multiple X-ray backscattering. The absorber (blue) is the source of the outgoing spherical wave. The wave is backscattered directly (red) or via several atoms (green).
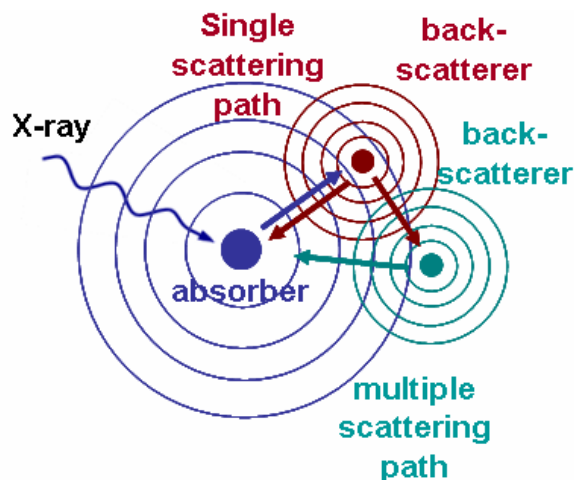
The scattering properties of the neighboring atoms (of j type) are described by parameters $F_j(k)$, $\lambda(k)$, and $\Phi_{ij}(k)$. $F_j(k)$ is the backscattering amplitude from each of the N_j neighboring atoms; $\Phi_{ij}(k)$ is the total phase-shift to the scattered photoelectron; the distance between absorber and backscatterer is given by R_j. The EXAFS phenomenon commonly is described by the "EXAFS equation" which readily accounts for the fine structure $\chi(k)$ and is used to simulate the spectrum in a fit procedure (Sayers *et al.* 1971) (Eq. 4).

$$\chi(k) = \sum_j N_j S_i(k) F_j(k) e^{2R_j/\lambda(k)} e^{2(k)^2 \sigma_j^2} \frac{sin[\,2kR_j + \Phi_{ij}(k)\,]}{kR_j^2} \qquad \textbf{(4)}$$

The term e^{-2R_j/λ_j} is due to inelastic losses in the scattering process (with $\lambda(k)$ being the mean free path). $S_i(k)$ is the amplitude reduction factor of the absorber. The mean-square disorder accounting for thermal vibrations (dynamic disorder) and static

disorder due to a certain spread R_j is given by the Debye-Waller parameter σ_j^2. $F_j(k)$, $\Phi_{ij}(k)$, $\lambda(k)$, and $S_i(k)$ usually is obtained from *ab initio* calculations employing a muffin-tin approximation of the potential landscape including the absorber and the backscatterers. By simulation N_j, N_i (number of backscatterers per metal atom), R_j, and σ_j^2 are determined.

Experimental setup for XAS and data processing

Figure 24 shows the experimental set-up at the BioXAS beamline at the EMBL (European Molecular Biology Laboratory at DESY, Hamburg, Germany) where the XAS experiments in this work have been performed.
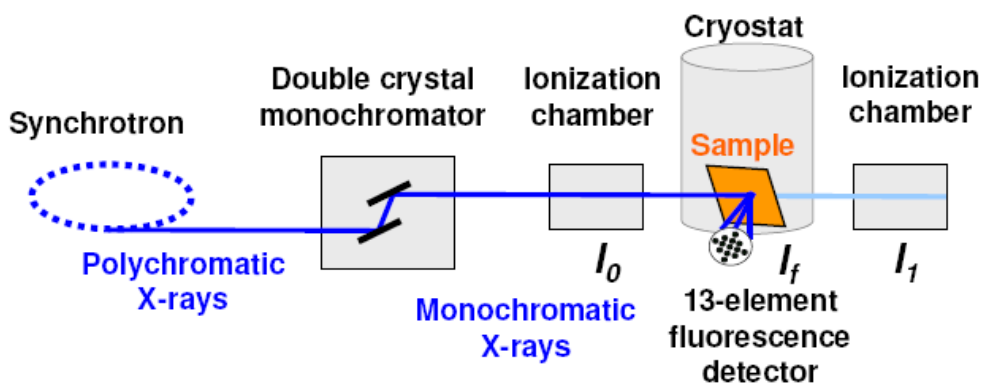

Figure 24: Simplified scheme of the experimental setup for XAS measurement sat the EMBL BioXAS beamline D2 (Deutsches Elektronen Synchrotron DESY, Hamburg, Germany). The polychromatic X-rays from the synchrotron are passed through a double crystal monochromator. The beam is focused to a spot of 1x5 mm on the sample in the cryostat. The emitted X-ray fluorescence is measured by a 13-element Ge solid state detector. I_0 and I_1 are measured by two ionization chambers placed as shown.

The synchrotron radiation source (Doris ring; HASYLAB; beamline D2) provides polychromatic X-rays. The beam passes through a double crystal monochromator (Si 111 crystals) and energy scans are performed by scanning of the monochromator (spot size on the sample of 1x5 mm). The sample is situated in a liquid He-cooled cryostat at 20 K. I_0 and I_1 are measured by two ionization chambers. The emitted X-ray fluorescence is monitored by a 13-element Ge solid-state detector. Bragg reflections from a static Si-crystal (Si 220) are recorded by scintillation counters simultaneously during the monochromator scan, permitting an absolute calibration of the energy axis (Pettifer *et al.* 1985).

The procedure of data processing, normalization of spectra, and extraction of the EXAFS oscillations from raw spectra as employed in our laboratory (Dau *et al.* 2003) is described in the following.

(1) An EXAFS spectrum representing I_f/I_0 (*E*) is recorded. Suitable spectra from the 13 detector channels are selected and averaged. The resulting spectrum is dead-time corrected and the energy axis is calibrated. The resulting spectra from several scans are summed.

(2) For normalization of the raw XAS spectrum the pre-edge background is eliminated by subtraction of a straight line. The spectrum is divided by a polynom (2nd or 3rd order) fitted through the EXAFS region to remove the background. The normalized spectrum represents the absorption per metal atom and is used for XANES analysis. XANES simulations were performed using the *ab initio* code FEFF 8.2. (Ankudinov *et al.* 1998).
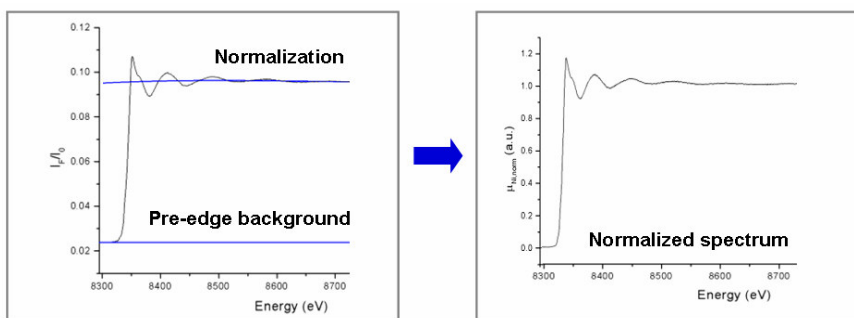
**(3)** For extraction of the EXAFS oscillations, the threshold energy E_0 of the absorption edge is selected. $\mu_0(E)$ is approximated by a smooth polynomial spline and the spectrum is divided by this spline. The EXAFS oscillations are centered around zero by subtraction of unity; E_0 is subtracted from the energy axis (Eq. 5).

$$\chi(E) = \frac{\mu_x(E) - \mu_0(E)}{\mu_0(E)} \qquad \textbf{(5)}$$
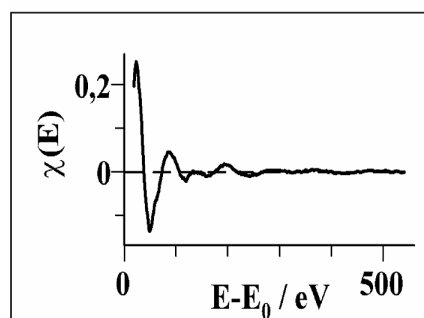
(4) The energy scale of the EXAFS spectrum is converted to a *k*-scale and the spectrum is reduced to ~200 data points, equidistant on the *k*-scale (Eq. 6, with $\hbar$ = Planck´s constant and *m* = mass of electron). For compensation of the damping of the EXAFS oscillations with increasing *k*, the spectrum is weighted by k^3.

$$k = \sqrt{\frac{2m}{\eta}\left(E - E_0\right)} \qquad \textbf{(6)}$$
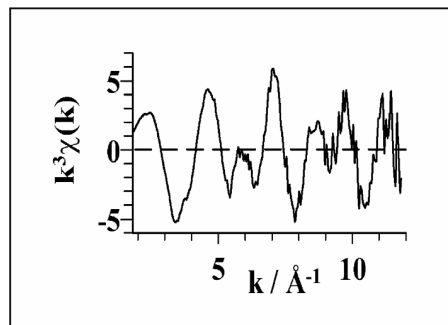
(5) For visualization of the absorber-backscatterer interactions in the sample, k^3-weighted data are Fourier-transformed from *k* to *R* space. The Fourier-transform (FT) allows to judge on approximate metal-ligand distances.
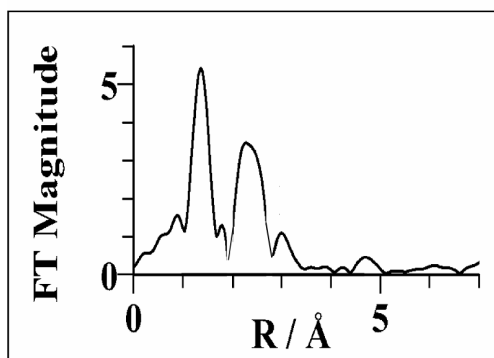
The EXAFS k^3-weighted oscillations are simulated using the EXAFS equation (Eq. 4). In this work the unfiltered k^3-weighted spectra were used for least-squares curve fitting with the in-house software SimX (Dittmer 1999) This program was also used for calculation of Fourier transforms employing fractional cosine window (usually 10 % at low and high *k*-side) to suppress side loops in the FT. EXAFS simulations were performed using complex backscattering amplitudes (phases) as calculated by FEFF 7 (Zabinsky *et al.* 1995). Further details of the data evaluation procedure are given in the respective material and methods sections in the following chapters.

Motivation of this work

Considerable progress has been achieved in recent years in the characterization of the molecular architecture and reaction cycle of hydrogenases. However, the mechanism of H_2 catalysis at the Ni-Fe site is only insufficiently understood. This holds in particular for the three O_2-tolerant hydrogenases of *R. eutropha*. The reasons, at the atomic level, for their O_2 and CO insensitive catalytic behavior are unclear. The following questions need to be addressed.

(1) What are the structural characteristics of the Ni-Fe sites of SH, RH, and MBH?

(2) How does the atomic structure and oxidation state of the Ni site change in the course of the catalytic reaction?

(3) What are the structural determinants of the oxygen-tolerant catalytic behavior at the atomic level?

(4) At which step of the catalytic cycle does hydrogen bind to the Ni-Fe site?

(5) What are the differences between energy-converting and sensory hydrogenases?

(6) How does signal transduction in H_2-sensor functions.

(7) What is the sequence of redox events involving the Ni-Fe and Fe-S cofactors?

In the investigations described in this thesis, several spectroscopic methods have been applied on the three Ni-Fe H_2ases of *R. eutropha*. A central role plays X-ray absorption spectroscopy (XAS) which was used to shed light on the architecture of the Ni-Fe active site and of the Fe-S clusters and to characterize intermediates occurring in the catalytic cycle. The results are compared to the situation in standard hydrogenases.

References

Ackrell, B. A. C., Asato, R. N. and Mower, H. F. (1966). "Multiple Forms of Bacterial Hydrogenases" *J. Bacteriol.* **92** (4): 828-838.

Adams, M. W. W. (1990). "The structure and mechanism of iron-hydrogenases" *Biochim. Biophys. Acta* **1020**: 115-145.

Adams, M. W. W., Mortenson, L. E. and Chen, J.-S. (1981). "Hydrogenase" *Biochim. Biophys. Acta* **594**: 105-176.

Albracht, S. P. J. (1994). "Nickel hydrogenases: in search of the active site" *Biochim. Biophys. Acta* **1188**: 167-204.

Albracht, S. P. J. and Hedderich, R. (2000). "Learning from hydrogenases: location of a proton pump and of a second FMN in bovine NADH--ubiquinone oxidoreductase (Complex I)" *FEBS Letters* **485** (1): 1-6.

Albracht, S. P. J., Van der Linden, E. and Faber, B. W. (2003). "Quantitative amino acid analysis of bovine NADH:ubiquinone oxidoreductase (Complex I) and related enzymes. Consequences for the number of prosthetic groups" *Biochim. Biophys. Acta* **1557** (1-3): 41-49.

Amara, P., Volbeda, A., Fontecilla-Camps, J. C. and Field, M. J. (1999). "A Hybrid Density Functional Theory/Molecular Mechanics Study of Nickel-Iron Hydrogenase: Investigation of the Active Site Redox States" *J. Am. Chem. Soc.* **121**: 4468-4477.

Ankudinov, A. L., Ravel, B., Rehr, J. J. and Conradson, S. D. (1998). "Real-space multiple-scattering calculation and interpretation of x-ray-absorption fine structure" *Phys. Rev. B* **12**: 7565-7576.

Benfatto, M., Della Longa, S. and Natoli, C. R. (2003). "The MXAN procedure: a new method for analysing the XANES spectra of metalloproteins to obtain structural quantitative information" *J. Synchrotron Rad.* **10**: 51-57.

Bernhard, M., Buhrke, T., Bleijlevens, B., DeLacey, A. L., Fernandez, V. M., Albracht, S. P. J. and Friedrich, B. (2001). "The H_2 Sensor of *Ralstonia eutropha*" *J. Biol. Chem.* **276** (19): 15592-15597.

Bernhard, M., Schwartz, E., Rietdorf, J. and Friedrich, B. (1996). "The *Alcaligenes eutrophus* Membrane-Bound Hydrogenase Gene Locus Functions Involved in Maturation and Electron Transport Coupling" *J. Bacteriol.* **178** (15): 4522-4529.

Brecht, M., Van Gastel, M., Buhrke, T., Friedrich, B. and Lubitz, W. (2003). "Direct Detection of a Hydrogen Ligand in the [NiFe] Center of the Regulatory H_2-Sensing Hydrogenase from *Ralstonia eutropha* in Its Reduced State by HYSCORE and ENDOR Spectroscopy" *J. Am. Chem. Soc.* **125**: 13075 - 13083.

Buhrke, T., Lenz, O., Porthun, A. and Friedrich, B. (2004). "The H_2-sensing complex of *Ralstonia eutropha*: interaction between a regulatory [NiFe] hydrogenase and a histidine protein kinase." *Mol. Microbiol.* **51** (6): 1677–1689.

Buhrke, T., Löscher, S., Lenz, O., Schlodder, E., Zebger, I., Andersen, L.-K., Hildebrandt, P., Dau, H., Friedrich, B. and Haumann, M. (2005). "Reduction of Unusual Iron-Sulfur Clusters in the H_2-sensing Regulatory Ni-Fe Hydrogenase from *Ralstonia eutropha* H16" *J. Bacteriol.* **280** (20): 19488–19495.

Burgdorf, T., Lenz, O., Buhrke, T., Van der Linden, E., Jones, A. K., Albracht, S. P. J. and Friedrich, B. (2005a). "[NiFe]-Hydrogenases of *Ralstonia eutropha* H16: Modular Enzymes for Oxygen-Tolerant Biological Hydrogen Oxidation" *J. Mol. Microbiol. Biotechnol.* **10**: 181-196.

Burgdorf, T., Löscher, S., Liebisch, P., Van der Linden, E., Galander, M., Lendzian, F., Meyer-Klaucke, W., Albracht, S. P. J., Friedrich, B., Dau, H. and Haumann, M. (2005b). "Structural and oxidation-state changes at a non-standard Ni-Fe site during activation of the NAD-reducing hydrogenase from *Ralstonia eutropha* detected by X-ray absorption-, EPR-, and FTIR-spectroscopy." *J. Am. Chem. Soc.* **127**: 576-592.

Burgdorf, T., Van der Linden, E., Bernhard, M., Yin, Q. Y., Back, J. W., Hartog, A. F., Muijsers, A. O., Koster, d. C. G., Albracht, S. P. J. and Friedrich, B. (2005c). "The Soluble NAD^+-Reducing [NiFe]-Hydrogenase from *Ralstonia eutropha* H16 Consists of Six subunits and Can Be Specifically Activated by NADPH" *J. Bacteriol.* **187**: 3122-3232.

Cammack, R. (1999). "Hydrogenase sophistication" *Nature* **397**: 214-215.

Cammack, R., Frey, M. and Robson, R. (2001). Hydrogen as a fuel: Learning from nature. London, New York, Taylor & Frances.

Cammack, R., Patil, D., Hatchikian, E. C. and Fernandez, V. M. (1987). "Nickel and iron-sulfur centres in *Desulfovobrio gigas* hydrogenase: ESR spectra, redox properties and interactions" *Biochim. Biophys. Acta* **912**: 98-109.

Carepo, M., Tierney, D. L., Brondino, C. D., Yang, T. C., Pamplona, A., Telser, J., Moura, I., Moura, J. J. and Hoffman, B. M. (2002). "^{17}O ENDOR Detection of a Solvent-Derived Ni-(OH$_x$)-Fe Bridge That Is Lost upon Activation of the Hydrogenase from *Desulfovibrio gigas*" *J. Am. Chem. Soc.* **124** (2): 281-286.

Dau, H., Liebisch, P. and Haumann, M. (2003). "X-ray absorption spectroscopy to analyze nuclear geometry and electronic structure of biological metal centers—potential and questions examined with special focus on the tetra-nuclear manganese complex of oxygenic photosynthesis" *Analyt. Bioanalyt. Chem.* **376** (5): 562 - 583.

De Lacey, A. L., Fernandez, V. M. and Rousset, M. (2005). "Native and mutant nickel–iron hydrogenases: Unravelling structure and function" *Coordination Chem. Rev.* **249**: 1596-1608.

De Lacey, A. L., Hatchikian, E. C., Volbeda, A., Frey, M., Fontecilla-Camps, J. C. and Fernandez, V. M. (1997). "Infrared-Spectroelectrochemical Characterization of the [NiFe] Hydrogenase of *Desulfovibrio gigas*" *J. Am. Chem. Soc.* **119**: 7181-7189.

Dittmer, J. (1999). *Linear-Dichroismus-Röntgenabsorptionsspektroskopie zum katalytischen Zyklus des wasserspaltenden Mangan-Komplexes der Photosynthese in Theorie und Experiment*, Ph. D. Thesis, Christian Albrechts-Universität

Erkens, A., Schneider, K. and Müller, A. (1996). "The NAD-linked soluble hydrogenase from *Alcaligenes eutrophus* H16: detection and characterization of EPR signals deriving from nickel and flavin" *J. Biol. Inorg. Chem.* **1**: 99-110.

Fernandez, V. M., Hatchikian, C. and Cammack, R. (1985). "Properties and Reactivation of two different deactivated forms of *Desulfovibrio gigas* hydrogenase" *Biochim. Biophys. Acta* **832**: 69-79.

Foerster, S., Stein, M., Brecht, M., Ogata, H., Higuchi, Y. and Lubitz, W. (2003). "Single Crystal EPR Studies of the Reduced Active Site of [NiFe] Hydrogenase from *Desulfovibrio vulgaris* Miyazaki F" *J. Am. Chem. Soc.* **125**: 83-93.

Frey, M. (1999). Nickel-Iron Hydrogenases: Structural and Functional Properties. Berlin, Heidelberg, Springer.

Frey, M. (2002). "Hydrogenases: Hydrogen-Activating Enzymes" *Chem. Biochem.* **3**: 153-160.

Friedrich, B., Buhrke, T., Burgdorf, T. and Lenz, O. (2005). "A hydrogen-sensing multiprotein complex controls aerobic hydrogen metabolism in *Ralstonia eutropha*" *Biochem. Soc. Trans.*: 97-101.

Garcin, E., Vernède, X., Hatchikian, E. C., Volbeda, A., Frey, M. and Fontecilla-Camps, J. C. (1999). "The crystal structure of a reduced [NiFeSe] hydrogenase provides an image of the activated catalytic center" *Structure Fold. Des.* **7** (5): 557-566.

Happe, R. P., Roseboom, W., Pierik, A. J., Albracht, S. P. J. and Bagley, K. A. (1997). "Biological activation of hydrogen" *Nature* **385** (6612): 126.

Haumann, M., Porthun, A., Buhrke, T., Liebisch, P., Meyer-Klaucke, W., Friedrich, B. and Dau, H. (2003). "Hydrogen-Induced Structural Changes at the Nickel Site of the Regulatory [NiFe] Hydrogenase from *Ralstonia eutropha* Detected by X-ray Absorption Spectroscopy." *Biochemistry* **42** (37): 11004-15.

Higuchi, Y., Ogata, H., Miki, K., Yasuoka, N. and Yagi, T. (1999). "Removal of the bridging ligand atom at the Ni-Fe active site of [NiFe] hydrogenase upon reduction with H2, as revealed by X-ray structure analysis at 1.4 A resolution" *Structure Fold. Des.* **7** (5): 549-56.

Higuchi, Y., Yagi, T. and Yasuoka, N. (1997). "Unusual ligand structure in Ni-Fe active center and an additional Mg site in hydrogenase revealed by high resolution X-ray structure analysis" *Structure* **5** (12): 1671-1680.

Hill, H. A. O., Sadler, P. J. and Thomson, A. J. (1999). Metal Sites in Proteins and Models. Berlin, Heidelberg, Springer.

Kaim, W. and Schwerderski, B. (2004). Bionaorgan. Chemie. Stuttgart, Germany, Teubner.

Kleihues, L., Lenz, O., Bernhard, M., Buhrke, T. and Friedrich, B. (2000). "The H_2 Sensor of *Ralstonia eutropha* Is a Member of the Subclass of Regulatory [NiFe] Hydrogenases" *J. Bacteriol.* **182** (10): 2716-2724.

Korbas, M., Vogt, S., Meyer-Klaucke, W., Bill, E., Lyon, E. J., Thauer, R. K. and Shima, S. (2006). "The iron-sulfur-cluster-free hydrogenase (Hmd) is a metalloenzyme with a novel iron binding motif" *J. Biol. Chem.*

Lenz, O., Bernhard, M., Buhrke, T., Schwartz, E. and Friedrich, B. (2002). "The Hydrogen-Sensing Apparatus in *Ralstonia eutropha*" *J. Mol. Microbiol. Biotech.* **4** (3): 255-262.

Lenz, O. and Friedrich, B. (1998). "A novel multicomponent regulatory system mediates H$_2$ sensing in *Alcaligenes eutrophus*" *Proc. Nat. Acad. Sci.* **95**: 12474-12479.

Lenz, O. and Friedrich, B. (2001). "Bakterielle Wasserstoff-Sensoren" *Biospektrum* **6**: 515-520.

Lenz, O., Gleiche, A., Strack, A. and Friedrich, B. (2005). "Requirements for Heterologous Production of a Complex Metalloenzyme: the Membrane-Bound [NiFe] Hydrogenase" *J Bacteriol.* **187** (18): 6590-6595.

Löscher, S., Burgdorf, T., Zebger, I., Hildebrandt, P., Dau, H., Friedrich, B. and Haumann, M. (2006). "Bias from H$_2$ Cleavage to Production and Coordination Changes at the Ni-Fe Active Site in the NAD$^+$-Reducing Hydrogenase from *Ralstonia eutropha*" *Biochem.* **45**: 11658-11665.

Löscher, S., Zebger, I., Andersen, L.-K., Hildebrandt, P., Meyer-Klaucke, W. and Haumann, M. (2005). "The structure of the Ni–Fe site in the isolated HoxC subunit of the hydrogen-sensing hydrogenase from *Ralstonia eutropha*" *FEBS Letters* **579**: 4287–4291.

Lyon, E. J., Shima, S., Buurman, G., Chowdhuri, S., Batschauer, A., Steinbach, K. and Thauer, R. K. (2004). "UV-A/blue-light inactivation of the 'metal-free' hydrogenase (Hmd) from methanogenic archaea" *Eur. J. Biochem.* **271**: 195-204.

Matias, P. M., Soares, C. M., Saraiva, L. M., Coelho, R., Morais, J., Legall, J. and Carrondo, M. A. (2001). "[NiFe] hydrogenase from Desulfovibrio desulfuricans ATCC 27774: gene sequencing, three-dimensional structure determination and refinement at 1.8 A and modelling studies of its interaction with the tetrahaem cytochrome c3" *J. Biol. Inorg. Chem.* **6** (1): 63-81.

Montet, Y. and Fontecilla-Camps, J. C. (1997). "Gas access to the active site of Ni–Fe hydrogenases probed by X-ray crystallography and molecular dynamics." *Nat. Struct. Biol.* **4**: 523-526.

Nicolet, Y., Piras, C., Leger, P., Hatchikian, C. E. and Fontecilla-Camps, J. C. (1999). "Desulfovibrio desulfuricans iron hydrogenase: the structure shows unusual coordination to an active site Fe binuclear center." *Struc. Fold. Des.* **7** (1): 13-23.

Ogata, H., Hirota, S., Nakahara, A., Komori, H., Shibata, N., Kato, T., Kano, K. and Higuchi, Y. (2005). "Activation Process of [NiFe] Hydrogenase Elucidated by High-Resolution X-Ray Analyses: Conversion of the Ready to the Unready State" *Structure* **13**: 1635-1542.

Pardo, A., De Lacey, A. L., Fernandez, V. M., Fan, H.-J., Fan, C. and Hall, M. B. (2006). "Density functional study of the catalytic cycle of nickel–iron [NiFe] hydrogenases and the involvement of high-spin nickel(II)" *J. Biol. Inorg. Chem.* **11**: 286-306.

Peters, J. W., Lanzilotta, W. N., Lemon, B. J. and Seefeldt, L. C. (1998). "X-ray Crystal Structure of the Fe-Only Hydrogenase (Cpl) from *Clostridium pasteurianum* to 1.8 Angstrom Resolution" *Science* **282**: 1853-1858.

Pettifer, R. F. and Hermes, C. (1985). "Absolute energy calibration of x-ray radiation from synchrotron sources" *J. Appl. Crystall.* **18** (6): 404-12.

Pierik, A. J., Hulstein, M., Hagen, W. L. and Albracht, S. P. J. (1998a). "A low-spin iron with CN and CO as intrinsic ligands forms the core of the active site in [Fe]-hydrogenases" *Eur. J. Biochem.* **258**: 572-578.

Pierik, A. J., Schmelz, M., Lenz, O., Friedrich, B. and Albracht, S. P. J. (1998b). "Characterization of the active site of a hydrogen sensor from *Alcaligenes eutrophus*" *FEBS Letters* **438**: 231-235.

Przybyla, A. E., Robbins, J., Menon, N. and Peck, H. D. J. (1992). "Structure-function relationships among the nickel-containing hydrogenases" *FEMS Microbiol. Rev.* **8** (2): 109-135.

Rehr, J. J. and Ankudinov, A. L. (2001). "Progess and challenges in the theory and interpretation of X-ray spectra" *J. Synchrotron Rad.* **8**: 61-65.

Sayers, D. E., Stern, E. A. and Lytle, F. W. (1971). "New technique for investigating noncrystalline structures: Fourier analysis of the extended X-ray-absorption fine structure" *Phys. Rev. Lett.* **27**: 1204-1207.

Schneider, K. and Schlegel, H. G. (1976). "Purification and properties of soluble hydrogenase from *Alcaligenes eutrophus* H 16" *Biochim. Biophys. Acta* **452**: 66-80.

Schwartz, L., Eilers, G., Eriksson, L., Gogoll, A., Lomoth, R. and Ott, S. (2006). "Iron hydrogenase active site mimic holding a proton and a hydride" *Chem. Comm.* **5**: 520-522.

Stein, M., Lenthe, E. v., Baerends, E. J. and Lubitz, W. (2001a). "Relativistic DFT calculations of the paramagnetic intermediates of [NiFe] hydrogenase. Implications for the enzymatic mechanism" *J. Am. Chem. Soc.* **123** (24): 5839-5840.

Stein, M. and Lubitz, W. (2001b). "DFT calculations of the elecronic structure of the paramagnetic states Ni-A, Ni-B and Ni-C of [NiFe] hydrogenase" *Phys. Chem. Chem. Phys.* **3**: 2668-2675.

Stein, M. and Lubitz, W. (2002). "Quantum chemical calculations of [NiFe] hydrogenase" *Curr. Opin. Chem. Biol.* **6**: 243-249.

Stein, M. and Lubitz, W. (2004). "Relativistic DFT calculation of the reaction cycle intermediates of [NiFe] hydrogenase: a contribution to understanding the enzymatic mechanism" *J. Inorg. Biochem.* **98**: 862-877.

Stephenson, M. and Strickland, L. H. (1931). "Hydrogenase: A Bacterial Enzyme Activating Molecular Hydrogen. I. The Properties of the Enzyme." *Biochem. J.* **25**: 205-214.

Teixeira, M., Moura, I., Xavier, A. V., Huynh, B. H., DerVartanian, D. V., Peck, H. D. J., Legall, J. and Moura, J. J. G. (1985). "Electron Paramagnetic Resonance Studies on the Mechanism of Activation and the Catalytic Cycle of the Nickel-containing Hydrogenase from *Desulfovibrio gigas*" *J. Biol. Chem.* **260** (15): 8942-8950.

Tran-Betcke, A., Warnecke, U., Böcker, C., Zaborosch, C. and Friedrich, B. (1990). "Cloning and nucleotide sequences of the genes for the subunits of NAD-reducing hydrogenase of *Alcaligenes eutrophus* H16." *J. Bacteriol.* **172** (6): 2920-2929.

Van der Linden, E., Bart, W., Faber, B., Bleijlevens, B., Burgdorf, T., Bernhard, M., Friedrich, B. and Albracht, S. P. J. (2004). "Selective release and function of one of the two FMN groups in the cytoplasmic NAD+-reducing [NiFe]-hydrogenase from *Ralstonia eutropha*" *Eur. J. Biochem.* **271**: 801-808.

Van Gastel, M., Stein, M., Brecht, M., Schröder, O., Lendzian, F., Bittl, R., Ogata, H., Higuchi, Y. and Lubitz, W. (2006). "A single-crystal ENDOR and density functional theory study of the oxidized states of the [NiFe] hydrogenase from *Desulfovibrio vulgaris* Miyazaki F" *J. Biol. Inorg. Chem.* **11**: 41-51.

Vignais, P. M., Billoud, B. and Meyer, J. (2001). "Classification and phylogeny of hydrogenases" *FEMS Microbiol. Rev.* **25** (4): 455-501.

Vignais, P. M. and Colbeau, A. (2004). "Molecular biology of microbial hydrogenases" *Curr Issues Mol Biol* **6**: 159-188.

Vincent, K. A., Cracknell, J. A., Lenz, O., Zebger, I., Friedrich, B. and Armstrong, F. A. (2005a). "Electrocatalytic hydrogen oxidation by an enzyme at high carbon monoxide or oxygen levels" *PNAS* **102** (47): 16951–16954.

Vincent, K. A., Parkin, A., Lenz, O., Albracht, S. P. J., Fontecilla-Camps, J. C., Cammack, R., Friedrich, B. and Armstrong, F. A. (2005b). "Electrochemical Definitions of O_2 Sensitivity and Oxidative Inactivation in Hydrogenases" *J Am Chem Soc.* **127**: 18179-18189.

Volbeda, A., Charon, M. H., Piras, C., Hatchikian, E. C., Frey, M. and Fontecilla-Camps, J. C. (1995). "Crystal structure of the nickel-iron hydrogenase from *Desulfovibrio gigas*" *Nature* **373** (6515): 556-557.

Volbeda, A., Martin, L., Cavazza, C., Matho, M., Faber, B. W., Roseboom, W., Albracht, S. P. J., Garcin, G., Rousset, M. and Fontecilla-Camps, J. C. (2005). "Structural differences between the ready and unready oxidized states of [NiFe] hydrogenases" *J. Biol. Inorg. Chem.* **10**: 239–249.

Zabinsky, S. I., Rehr, J. J., Aukudinov, A., Albers, R. C. and Eller, M. J. (1995). "Multiple-scattering calculations of x-ray-absorption spectra" *Phys. Rev. B* **52** (4): 2995-3009.